SCIENCE CHINA Materials ARTICLES

mater.scichina.com link.springer.com

Published online 22 March 2019 | https://doi.org/10.1007/s40843-019-9409-1
Sci China Mater 2019, 62(8): 1169–1176

Small onion-like BN leads to ultrafine-twinned cubic BN

Kun Luo[1,2†], Yang Zhang[1,2†], Dongli Yu[1†], Baozhong Li[1], Wentao Hu[1], Yong Liu[2], Yufei Gao[1], Bin Wen[1], Anmin Nie[1], Zhisheng Zhao[1*], Bo Xu[1], Xiang-Feng Zhou[1], Yongjun Tian[1] and Julong He[1*]

ABSTRACT **Nanotwinned cubic boron nitride (nt-cBN) with remarkable hardness, toughness, and stability has attracted widespread attention due to its distinct scientific and industrial importance. The key for nt-cBN synthesis is to adopt an onion-like BN (oBN) nano-precursor and induce phase transition under high pressure. Here, we found that the size change of oBN used greatly affected the mechanical performance of products. With the precursor size decreasing from ~320 to 90 nm, the Vickers hardness of nanostructured products improved from 61 to 108 GPa, due to the fact that large oBN nanoparticles possessed more flattened, orderly and graphite-like shell layers, in sharp contrast to the highly wrinkled and imperfect layers in small-diameter nanoparticles, thus resulting in the apparent reduction of ultrafine-twin substructure in the synthetic products. This study reveals that only small oBN precursor could produce complete ultrafine nt-cBN with outstanding performance. A practical route was proposed to further improve the performance of this important material.**

Keywords: onion-like BN, nanotwinned cBN, size effect, hardness, high pressure and high temperature

INTRODUCTION

Cubic boron nitride (cBN) is a widely used superhard material that plays an irreplaceable role in modern industry [1]. In addition to its high hardness, its excellent thermal and chemical stabilities make cBN the best material for cutting ferrous and carbide-forming hard substances where diamond completely fails. In comparison with cBN single crystals, the polycrystalline cBN sintered with metal or ceramic binder shows isotropic property, excellent toughness and easy scalability [2,3]. The hardness of this type of cemented polycrystalline cBN is 33–45 GPa [2,3], which is higher than those of heavy transition metal carbides or nitrides but much lower than that of diamond (~100 GPa) [4], thus limiting its application to some extent. For decades, scientists and industrialists aimed to further improve the mechanical performances of polycrystalline cBN [5–9].

Nano-structuring is an effective approach to strengthen the mechanical properties of materials according to the Hall–Petch law [10,11]. Recently, the nanopolycrystalline cBN material has been synthesized by direct transition of pyrolytic graphite-like BN (pBN) at high pressure of ~20 GPa and temperature of ~1,870 K. This type of polycrystalline bulk has an average nanograin size of as small as ~14 nm, thus resulting in a remarkably high Vickers hardness of 85 GPa [5,6]. Further refinement of the grain is nearly impossible due to the high synthesis temperature, which promotes the growth of nanograins. Another effective way is to achieve nanotwinning, because the coherent twin boundaries possess the excess energy that is typically about one order of magnitude lower than that of grain boundaries [12]. However, it is also very difficult to obtain an entire or high-density nanotwinning microstructure in ceramics. With the highly puckered and defective onion-like boron nitride (oBN) nanoparticles as precursor, the nanopolycrystalline cBN with ubiquitous ultrafine nanotwin substructure, called nanotwinned cBN (nt-cBN), has been successfully synthesized under pressures of 12–15 GPa and temperature of 1,800–1,950°C [9]. The synthetic nt-cBN displays ultrafine nanotwins with average twin thickness of

[1] Center for High Pressure Science (CHiPS), State Key Laboratory of Metastable Materials Science and Technology, Yanshan University, Qinhuangdao 066004, China
[2] Hebei Key Laboratory of Microstructural Material Physics, School of Science, Yanshan University, Qinhuangdao 066004, China
[†] These authors contributed equally to this paper.
[*] Corresponding authors (emails: zzhao@ysu.edu.cn (Zhao Z); hjl@ysu.edu.cn (He J))

3.8 nm, leading to the remarkable enhancement of Vickers hardness up to 108 GPa (as hard as natural diamond crystal), fracture toughness of 12.7 MPa $m^{1/2}$ (3–4 times that of commercial single-crystal cBN), and oxidization temperature of ~1,294°C (~200°C higher than single-crystal cBN) [9]. Following the same principle, the nanotwinned diamond (nt-diamond) with unprecedented hardness—two times higher than that of single crystal diamond—has also been synthesized by compressing onion carbon [13,14]. The continuous hardening to deep nanoscale for nt-cBN and nt-diamond can be well-explained with Hall–Petch and quantum confinement effects [15].

The microstructures of high-pressure quenched materials are highly dependent on the initial precursors, pressure, and temperature as well as the compression history, which are determined by both kinetics and thermodynamics. Apparently, using oBN nanoparticles as precursor is the key to form high-performance nt-cBN with ubiquitous, interpenetrating ultrafine nanotwins [9]. Detailed transmission electron microscopy (TEM) observation reveals that oBN nanoparticles with the size of 30–150 nm and numerous puckered layers with high concentration of stacking faults inside could transfer to cBN with dense lamellar {111} ultrafine twins in the nanograins [9]. In comparison, graphite-like hBN and pBN with more flattened layers readily form nanograined cBN but hardly form the ubiquitous nanotwin microstructure [5,6]. Therefore, the structural features of starting materials would determine the microstructure of the transformed products in BN system [5,6,8,9,16,17]. In addition, the size effect of precursor is important, e.g., TiO_2 anatase nanocrystals exhibit strong size-dependent phase selectivity at high pressure [18]. This effect seems straightforward but the intrinsic mechanisms are distinct for different material systems. The intrinsic mechanism of nt-cBN material has not been thoroughly investigated. In this work, oBN materials with different nanoparticle sizes were prepared, and then subjected to the appropriate synthesis condition to obtain nanopolycrystalline cBN. The significant influence of nanoparticle size of precursor on mechanical properties of the final products was analyzed by multiple characterization methods. This study provides a potential route to fabricate high-performance nt-cBN material.

EXPERIMENTAL SECTION

Preparation of different-size oBN precursors

The oBN nanopowder with a wide particle size of about 30–400 nm was prepared by chemical vapor deposition [19], and then a centrifuge (Heraeus Multifuge X3R centrifuge, Thermo Fisher Scientific) was used to divide the methanol-dispersed, prefabricated nanopowder into oBN precursors of four sizes with 30–150 nm [9] (average ~90 nm, labeled as oBN90), 100–150 nm (average ~120 nm, labeled as oBN120), 150–250 nm (average ~200 nm, labeled as oBN200), and 250–400 nm (average ~320 nm, labeled as oBN320).

Synthesis of nanopolycrystalline cBN bulk products

The oBN precursor was prepressed into a pellet with 2.5 mm in diameter and 2 mm in height, and then subjected to high pressure and high temperature (HPHT), identical to previous report by Tian *et al.* [9]. The standard compress 10/5 sample assembly was used, which consisted of a 10-mm spinel ($MgAl_2O_4$) + MgO octahedron with a Re heater and a $LaCrO_3$ thermal insulator. Temperature was measured using a type W-Re thermocouples, and pressure was estimated from previously obtained calibration curves at different temperatures [20]. Then, the nanopolycrystalline cBN bulk samples (labeled as cBN90, cBN120, cBN200, and cBN320, respectively) were synthesized by a 10-MN two-stage large-volume multi-anvil system [21] under pressure of 15 GPa, temperature of 1,800°C, and holding time of 30 min. Recovered samples were about 2 mm in diameter and 1.5 mm in height and polished for further analysis.

XRD, Raman and TEM analyses

The phases were identified through X-ray diffraction (XRD) (Bruker D8 Discover) with Cu Kα radiation (λ = 0.15406 nm, 40 kV, 40 mA). Raman spectrum was obtained using a Horiba Jobin–Yvon LabRAM HR-Evolution Raman microscope and a laser radiation of 532 nm. The morphologies of the precursors were characterized by TEM (JEM-2010) with an accelerating voltage of 200 kV. High-resolution TEM (HRTEM) images were characterized by Titan ETEM G2 with an accelerating voltage of 300 kV. For better analysis, the orthogonal sample pieces (5 μm×8 μm×0.1 μm) were prepared using focused ion beam (FIB, FEI SCIOS). The grain distribution of the pieces was counted from bright-field TEM images (Talos F200X).

Hardness and fracture toughness measurements

The indentation test was performed on a polished sample surface by using a microhardness tester (KB 5 BVZ). The adopted loading time was 30 s, and a 20-s dwell time was kept at the peak load. For each sample, at least 5 in-

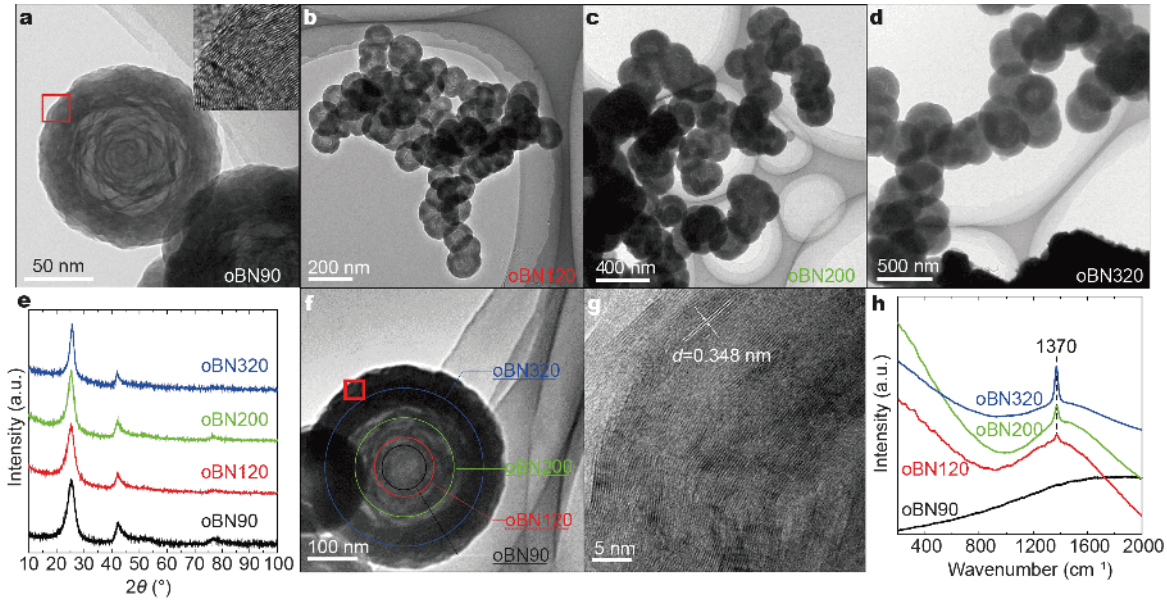

Figure 1 Characterization of the starting oBN nanoparticles with different size. (a–d), TEM images of oBN90, oBN120, oBN200 and oBN320, showing the size change. The inset in (a) is the HRTEM image corresponding to the marked white-box area, showing numerous defects including puckering, bending and stacking faults in the shell layers of oBN90. (e) XRD patterns of oBN precursors. Their interlayer spacings are 0.351–0.348 nm, which is larger than the (002) reflection of hBN 0.3328 nm. (f) Schematic of size division in a large oBN nanoparticle. The large oBN can be simply seen as the small one packaged with extra BN shells possessing smaller curvatures. (g) HRTEM image corresponding to the marked red-box position in (f), showing a more flattened, ordered and less-defective graphite-like microstructure in the shell layers of large oBN, in sharp contrast to the rich defects of oBN90 (see inset of (a)). (h) Raman spectra of oBN precursors. Above the size of 120 nm, a sharp Raman peak at about 1,370 cm^{-1} is present, which corresponds to the E_{2g} mode of hBN.

dentations were performed at different locations with increasing loads of 0.98–9.8 N. The Vickers hardness (H_v) was determined from $H_v = 1854.4F/L^2$, where F is the applied load and L is the mean of the two diagonals of the indentation in micrometers (μm). Five hardness indentations were obtained at each load, and the hardness was determined from the asymptotic hardness region. The radial cracks formed in the bulk sample at load of 9.8 N were used to calculate the fracture toughness (K_{IC}) with the equation [22,23] $K_{IC} = 7.42 \times 10^{-2} F/L^{1.5}$, where L (μm) is the average length of the radial cracks measured from the indent center and F (N) is the applied load, respectively. The Knoop hardness (H_k) at a load of 4.9 N was also measured with the same parameters for comparison. The H_k is defined as the applied load F (N) divided by the projected area of the indentation after unloading: $H_k = 14229F/d^2$, where d is the major diagonal (longer axis) length of the Knoop indentation in μm. The hardness indentations were imaged by the scanning electron microscope (SEM) (FEI SCIOS). To get clear indentation and crack with SEM, the polished sample surface was firstly sprayed with thin Pt of about 5 nm thickness before hardness testing.

RESULTS AND DISCUSSION

To obtain oBN precursors of various sizes, we firstly prepared nanopowder with grain size of 30–400 nm by chemical vapor deposition [19], and then four kinds of oBN precursors were separated by high-speed centrifuge: oBN90, oBN120, oBN200 and oBN320. oBN90 was prepared in accordance with our previous work [9]. The microstructures of the four oBN precursors were characterized by HRTEM, as shown in Fig. 1a–d. Although each precursor has a similar Matryoshka-doll-like onion structure, their sizes and internal microstructures are distinct, e.g., small oBN90 and large oBN320 (Fig. 1a and g). The shell layers of large-diameter oBN are more flattened, ordered and less defective due to the smaller external curvature, compared with those of small-diameter oBN. Theoretically, with the increase of particle size, the outermost shell of oBN is closer to the general graphite-like hBN layers [24]. To further characterize the precursors, XRD and Raman spectra were performed (Fig. 1e and h). With the increase in particle size, no appreciable difference of XRD patterns was observed, and only the full-width at half-maximum (FWHM) of the diffraction peak at $2\theta \approx 25°$ became slightly narrow (Fig. 1e). Given

that Raman vibrational modes are more sensitive to structural changes, there is a large discrepancy between the four oBN precursors (Fig. 1h). For oBN120, oBN200, and oBN320, a Raman peak at about 1370 cm^{-1} corresponding to E_{2g} mode of hBN [25,26] becomes more visible and sharper with increasing grain sizes, indicating that the outer shell layers of large oBN nanoparticles become similar to that of hBN. The precursors with different-size have different microstructures, which would affect the formed products.

The oBN precursors with different sizes were pressed into pellets with 2.5 mm in diameter and 2 mm in height, and subjected to HPHT (i.e., 15 GPa and 1,800°C) at a multi-anvil apparatus. After reaching ambient pressure and temperature, the compact pillars of polycrystalline cBN formed and were analyzed by XRD and Raman (Fig. 2). The XRD data show that cBN90 and cBN120 corresponding to oBN90 and oBN120 precursors are pure cubic phases. For the cBN200 and cBN320, a small amount of wurtzite BN (wBN) phase appears (Fig. 2a). In addition, the fingerprint Raman peak of wBN [27] also appears at 964 cm^{-1} for both cBN200 and cBN320 (Fig. 2b). The wBN usually forms during the transformation of pBN [5,6] and hBN [16,28] with more perfect graphite-like layers, due to the structural similarity between hBN and wBN. The direct linkage of AaAa stacked hBN would form wBN. Therefore, the residual wBN phase in cBN200 and cBN320 is highly possible from the transformation of ordered shell layers [5,6,16,28], and the phase difference in the products is caused by the diversity of the oBN precursors.

The microstructures of cBN were further investigated with TEM images, as shown in Fig. 3a, c. To visualize the grain and twin in a large field, bright-field images were firstly taken from the thin sample chips cut by focused-ion beam (FIB) technique (Fig. 3a). The statistical grain sizes are about 25–156 nm (average ~62 nm), 32–178 nm (average ~78 nm), and 35–252 nm (average ~109 nm) for cBN120, cBN200, and cBN320, respectively (Fig. 3b). The grain sizes of products gradually increase, but the relative contents of twins inside seem to reduce, with the increase in grain size of the used oBN precursors. HRTEM analysis on specific grains shows that some large grains in products have either few twins inside or twins with large width. Twin and grain boundaries as well as stacking faults are along the [101] axis in specific grains (Fig. 3c), and the insets show the relatively large twins in grains, thus resulting in the decrease of ultrafine twins. The distribution of twin thickness in each product was further counted in twin-rich grains (Fig. 3d). The average twin thickness for cBN120, cBN200, and cBN320 is 4.6–5.8 nm, which is larger than that (~3.8 nm) in cBN90 [9]. The additional large twins have a thickness range of 20–65 nm, and the large twins in grains would severely limit the area of small twins. As a result, the large nanograins and wide subtwins form due to the transitions of graphite-like shell layers in large-sized oBN precursors. Notably, there is no wide twins in cBN90 (thickness <15 nm), suggesting the ultrafine-twins inside. This finding is consistent with previous report on the use of regular graphite-like BN as precursors merely generating the ng-cBN [5–8,29], although twin domains are occasionally observed during the growth of cBN single crystals as extra substructures [24,30–32]. In comparison, the highly wrinkled and curved layers in small oBN (or core layers in large oBN) are easily transformed into ultrafine-twinned microstructure. Furthermore, smaller raw materials produced thinner twins.

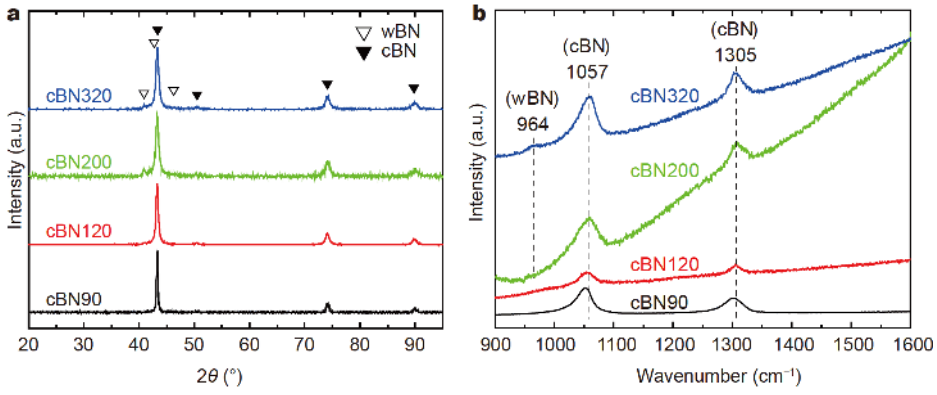

Figure 2 XRD patterns (a) and Raman spectra (b) of the cBN synthesized from different oBN precursors. A little residual wBN phase presents in cBN200 and cBN320 spectra. The (002) reflection of wBN and (111) of cBN are very close, thereby widening the XRD peak around 43° for cBN200 and cBN320, compared with that of cBN90 and cBN120.

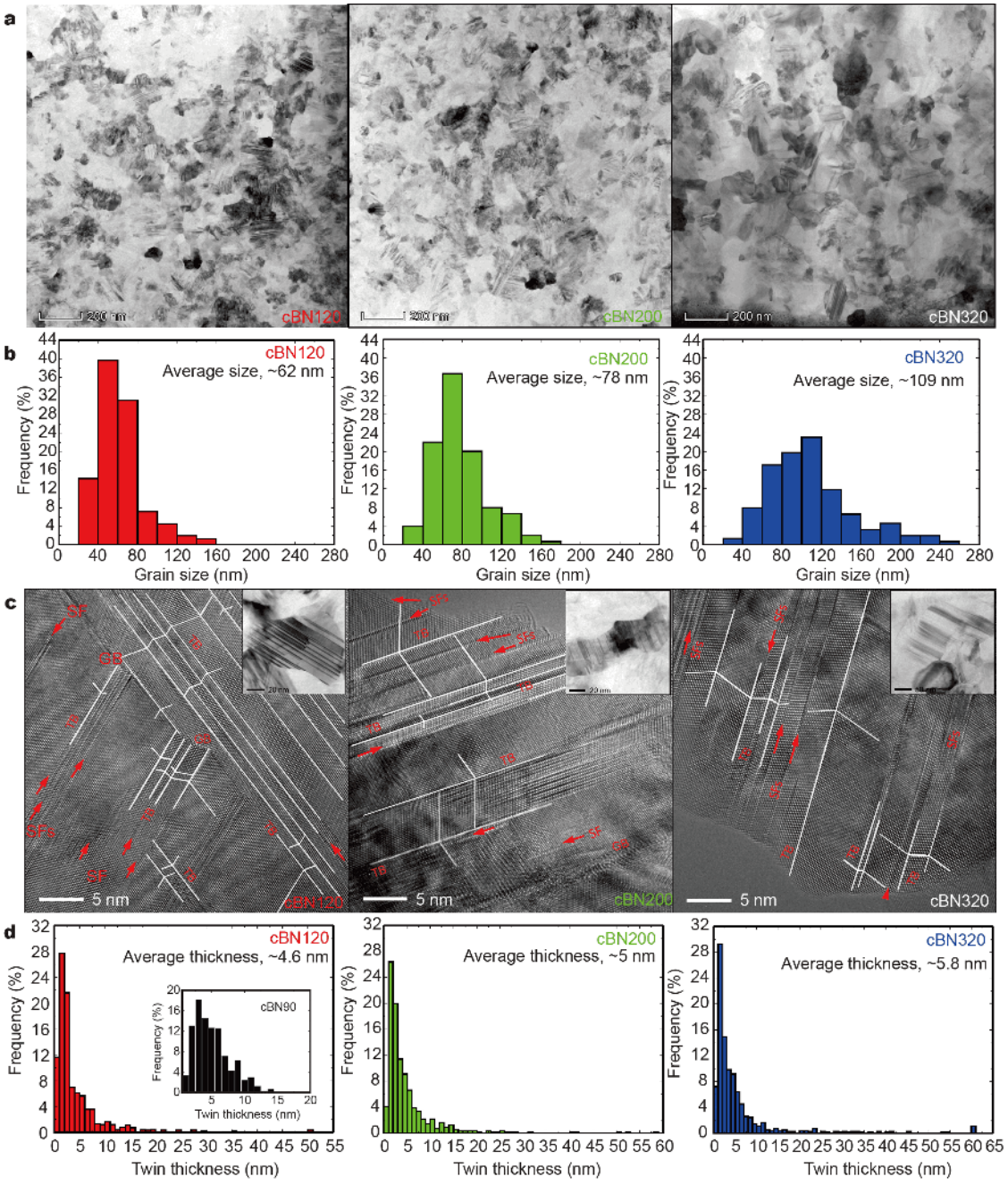

Figure 3 Microstructure of the synthetic cBN. Bright-field TEM images (a) and the statistical distribution of grain size (b) of cBN120 (left), cBN200 (middle), and cBN320 (right). (c) Corresponding HRTEM images along the [101] zone axis from the screened nanograins including fine twin substructure. The insets show the existence of relatively large twins in grains, thus decreasing the content of ultrafine twins inside. Twin boundaries (TBs), grain boundaries (GB), and stacking faults (SF) are marked by white lines or red arrows in the images. (d) Statistical distribution of the twin thickness. The inset shows the twin distribution of cBN90 [9]. A total of 838, 572, and 749 twins were measured to determine the twin thickness distribution for cBN120, cBN200, and cBN320, respectively.

The different microstructures of the synthetic cBN would lead to their distinct mechanical properties. Vickers hardness (H_v) was measured with a standard square-pyramidal diamond indenter. The variations of H_v with respect to a series of applied loads were recorded (Fig. 4). The asymptotic hardness values of cBN90, cBN120, cBN200, and cBN320 were estimated to be 108 (10) [9], 80(2.9), 66(3.1), and 61(1.1) GPa, respectively,

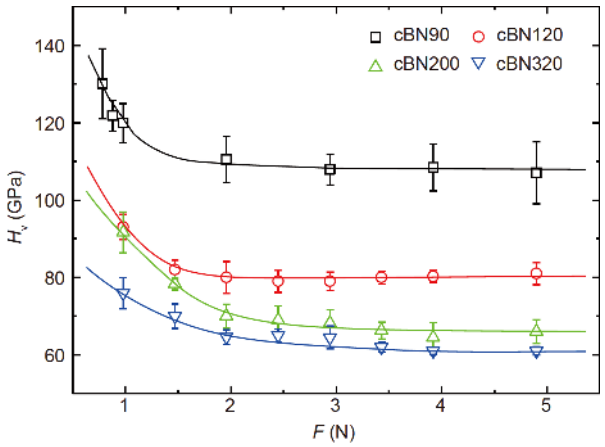

Figure 4 H_v of the produced cBN bulk materials as a function of applied loads. The H_v reaches asymptotic value when the applied load exceeds 3 N. Error bars indicate s.d. (n=5). The asymptotic H_v of cBN90, cBN120, cBN200, and cBN320 are 108(10) [9], 80(2.9), 66(3.1), and 61(1.1) GPa, respectively.

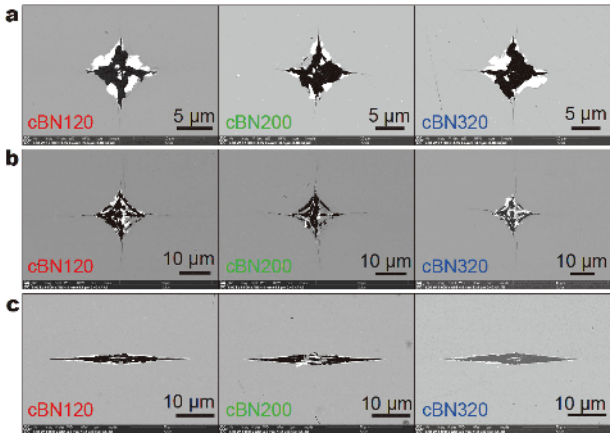

Figure 5 SEM images of indentations formed on cBN120, cBN200, and cBN320 bulk materials. (a) Vickers indentations at a load of 4.9 N. (b) Vickers indentations with cracks generated at a load of 9.8 N used for fracture toughness calculation. (c) Knoop indentations at a load of 4.9 N. To get clear indentation and crack during SEM observation, the polished sample surface was firstly sprayed with thin Pt of about 5 nm thickness before hardness testing.

before large cracks produced [33,34] (see the typical Vickers indentations in Fig. 5a). The Vickers hardness of cBN200 and cBN320 are close to that of nanopolycrystalline cBN (~70–50 GPa) with corresponding grain sizes of 20–400 nm containing less ultrafine twins inside [5,6,15,35].

In addition, Knoop hardness of cBN90, cBN120, cBN200, and cBN320 were also measured to be 78(3.8) [9], 51(0.4), 49(0.7), and 46(0.9) GPa, respectively. The imprints were accurately measured with SEM (Fig. 5c). Notably, the H_v is higher than H_k, due to different indenter geometries and calculation method [36]. Nonetheless, the H_k of cBN90 and cBN120 is clearly higher than the H_k of ng-cBN bulk materials, which are ~ 45 GPa [35]. We also estimated the fracture toughness K_{IC} of cBN90, cBN120, cBN200, and cBN320 to be 12.7 [9], 10.1 (2.6), 9.4(2.1), and 7.3(1.4) MPa $m^{1/2}$, respectively. Fig. 5b presents the indentations with large cracks generated at a load of 9.8 N for fracture toughness calculation. The above result demonstrates that the mechanical properties of the synthetic cBN are weakened with the increase in size of oBN precursors. Therefore, only small-sized oBN precursors can transform to the high-performance polycrystalline cBN composed of a high-density ultrafine nanotwin substructure.

Common polycrystalline metal materials can be continuously hardened according to Hall–Petch law by decreasing the grain size to up to ~10 nm. Below that critical size, the hardening mechanism may change the dislocation-related behavior to grain boundary sliding, thus decreasing the hardness. In the current case, the synthetic polycrystalline cBN has grain size above the critical size of 10 nm, which indicates that Hall–Petch law remains valid. Moreover, owing to the unique onion-like precursors, the ultrafine-twin substructure can form in each nanograin, which further impedes dislocation slip and increases the hardness. Additionally, the grain and twin boundaries are very secure due to the strong B–N covalent bonds in grain boundaries. The hardening mechanism in polycrystalline covalent material should be different from that in metal materials at nanoscale. Considering Hall–Petch and quantum confinement effects together, the hardness of a well-sintered polycrystalline cBN can be evaluated as follows: $H_V = H_{HP} + H_{qc} = H_0 + K_{HP}D^{-1/2} + K_{qc}D^{-1}$, where H_0 is the Vickers hardness of a perfect single crystal, and D indicates the average grain size or twin thickness (nm) [9,15]. For polycrystalline cBN, H_0, K_{HP}, and K_{qc} are 39 GPa, 126 GPa $nm^{1/2}$, and 130.7 GPa nm, respectively, as estimated from experimental data [5,6,9]. For pure nanograined cBN without subtwins inside, its theoretical Vickers hardness can only reach to 57 GPa with grain size decreased to 60 nm (the average grain size of cBN90 [9]). By comparison, the full nanotwinned cBN would have a theoretical Vickers hardness of as high as 134 GPa with the average twin as thin as 4 nm (the average twin thickness of cBN90 [9]). The experimental Vickers hardness is 108 GPa[9], which is slightly lower than theoretical value. Thus, the hardness of polycrystalline cBN is affected by three factors: nanograin size, nanotwin

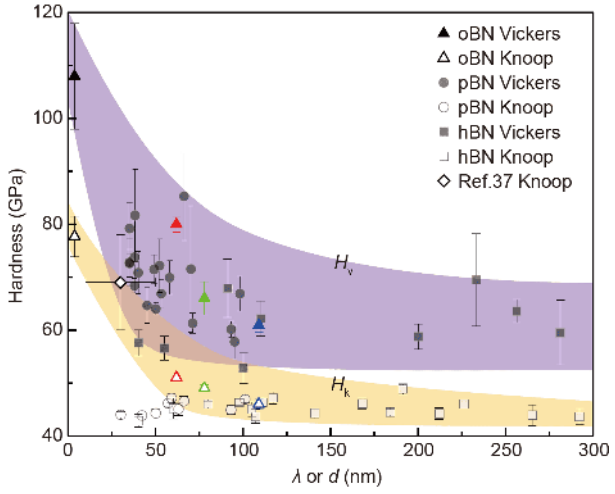

Figure 6 H_v and H_k as a function of average grain size (d) or twin thickness (λ) for polycrystalline cBN bulk materials synthesized with oBN (triangles), pBN (circles), and hBN (squares). Experimental data of the synthetic materials (triangles) and ng-cBN materials [35,37] (circles, squares, and diamond) are shown. Filled symbols: H_v, unfilled symbols: H_k. Load: 4.9 N.

thickness, and proportion of ultrafine-twin. In present work, both the Vickers and Knoop hardness results show that the hardness gradually increases with the decrease of grain size and twin thickness (Fig. 6), which complies with Hall–Petch law.

CONCLUSIONS

The size, shape, and microstructure of precursor would affect the products during chemical reactions or phase transitions. However, the direct relationships are difficult to confirm and the mechanisms need detailed analysis. With respect to microstructure, the relationship between the different-sized oBN precursors and the corresponding products was investigated by XRD, Raman, and TEM. HRTEM shows that the large oBN precursors having the more regular and ordered shell layers are preferred to form the nanopolycrystalline cBN with large nanograins and less ultrafine twins inside. Only the small oBN with highly defective and curved layers can produce high-performance, more complete nt-cBN with ubiquitous ultrafine subtwins in nanograins. The current investigation reveals that the size change of oBN precursors results in large microstructure difference in the precursors, which is unusual in nanomaterials. This kind of distinct precursors leads to significant change in microstructure and performance of the produced nanopolycrystalline cBN bulk materials. The mechanical properties of nt-cBN can be improved by using finer oBN precursors. Theoretically, the hardness of nt-cBN with entire ultrafine-twin microstructure can reach as high as 200 GPa, i.e., twice the hardness of natural diamond crystal, when the twin thickness is reduced to 2 nm. Such achievement would inspire numerous studies for the synthesis of better nt-cBN materials through further reduction of the size of oBN precursors.

Received 22 January 2019; accepted 22 February 2019; published online 22 March 2019

1 Wentorf Jr. RH. Cubic form of boron nitride. J Chem Phys, 1957, 26: 956
2 Liew WYH, Yuan S, Ngoi BKA. Evaluation of machining performance of STAVAX with PCBN tools. Int J Adv Manufact Tech, 2004, 23: 11–19
3 Wentorf RH, Devries RC, Bundy FP. Sintered superhard materials. Science, 1980, 208: 873–880
4 Krauss AR, Auciello O, Gruen DM, *et al.* Ultrananocrystalline diamond thin films for MEMS and moving mechanical assembly devices. Diamond Related Mater, 2001, 10: 1952–1961
5 Dubrovinskaia N, Solozhenko VL, Miyajima N, *et al.* Superhard nanocomposite of dense polymorphs of boron nitride: Noncarbon material has reached diamond hardness. Appl Phys Lett, 2007, 90: 101912
6 Solozhenko VL, Kurakevych OO, Le Godec Y. Creation of nanostuctures by extreme conditions: High-pressure synthesis of ultrahard nanocrystalline cubic boron nitride. Adv Mater, 2012, 24: 1540–1544
7 Sumiya H, Uesaka S, Satoh S. Mechanical properties of high purity polycrystalline cBN synthesized by direct conversion sintering method. J Mater Sci, 2000, 35: 1181–1186
8 Dub SN, Petrusha IA. Mechanical properties of polycrystalline cBN obtained from pyrolytic gBN by direct transformation technique. High Pressure Res, 2006, 26: 71–77
9 Tian Y, Xu B, Yu D, *et al.* Ultrahard nanotwinned cubic boron nitride. Nature, 2013, 493: 385–388
10 Petch NJ. The cleavage strength of polycrystals. J Iron Steel Inst, 1953, 174: 25–28
11 Hall EO. The deformation and ageing of mild steel: III Discussion of results. Proc Phys Soc B, 1951, 64: 747–753
12 Lu L, Chen X, Huang X, *et al.* Revealing the maximum strength in nanotwinned copper. Science, 2009, 323: 607–610
13 Huang Q, Yu D, Xu B, *et al.* Nanotwinned diamond with unprecedented hardness and stability. Nature, 2014, 510: 250–253
14 Hu W, Wen B, Huang Q, *et al.* Role of plastic deformation in tailoring ultrafine microstructure in nanotwinned diamond for enhanced hardness. Sci China Mater, 2017, 60: 178–185
15 Zhao Z, Xu B, Tian Y. Recent advances in superhard materials. Annu Rev Mater Res, 2016, 46: 383–406
16 Sumiya H, Harano K, Ishida Y. Mechanical properties of nanopolycrystalline cBN synthesized by direct conversion sintering under HPHT. Diamond Related Mater, 2014, 41: 14–19
17 Kurakevych OO, Solozhenko VL. High-pressure design of advanced BN-based materials. Molecules, 2016, 21: 1399
18 San-Miguel A. Nanomaterials under high-pressure. Chem Soc Rev, 2006, 35: 876
19 Tang C, Bando Y, Huang Y, *et al.* Synthetic routes and formation mechanisms of spherical boron nitride nanoparticles. Adv Funct Mater, 2008, 18: 3653–3661

20 Leinenweber KD, Tyburczy JA, Sharp TG, *et al.* Cell assemblies for reproducible multi-anvil experiments (the COMPRES assemblies). Am Miner, 2012, 97: 353–368
21 Wang Y, Rivers M, Sutton S, *et al.* The large-volume high-pressure facility at GSECARS: A "Swiss-army-knife" approach to synchrotron-based experimental studies. Phys Earth Planet Inter, 2009, 174: 270–281
22 Solozhenko VL, Dub SN, Novikov NV. Mechanical properties of cubic BC_2N, a new superhard phase. Diamond Related Mater, 2001, 10: 2228–2231
23 Evans AG, Charles EA. Fracture toughness determinations by indentation. J Am Ceramic Soc, 1976, 59: 371–372
24 He LL, Akaishi M, Horiuchi S. Structural evolution in boron nitrides during the hexagonal-cubic phase transition under high pressure at high temperature. Microsc Res Tech, 1998, 40: 243–250
25 Xiong C, Tu W. Synthesis of water-dispersible boron nitride nanoparticles. Eur J Inorg Chem, 2014, 19: 3010–3015
26 Zhao Z, Yang Z, Wen Y, Wang Y. Facile synthesis and characterization of hexagonal boron nitride nanoplates by two-step route. J Am Ceram Soc, 2011, 94: 4496–4501
27 Sachdev H. Influence of impurities on the morphology and Raman spectra of cubic boron nitride. Diamond Related Mater, 2003, 12: 1275–1286
28 Huang JY, Zhu YT. Advances in the synthesis and characterization of boron nitride. DDF, 2000, 186-187: 1–32
29 Britun VF, Kurdyumov AV. Mechanisms of martensitic transformations in boron nitride and conditions of their development. High Pressure Res, 2000, 17: 101–111
30 Zheng S, Zhang R, Huang R, *et al.* Structure and energetics of nanotwins in cubic boron nitrides. Appl Phys Lett, 2016, 109: 081901
31 Chen CL, Huang R, Wang Z, *et al.* Microstructures and grain boundaries of cubic boron nitrides. Diamond Related Mater, 2013, 32: 27–31
32 Oku T, Hiraga K, Matsuda T, *et al.* Twin structures of rhombohedral and cubic boron nitride prepared by chemical vapor deposition method. Diamond Related Mater, 2003, 12: 1138–1145
33 Tian Y, Xu B, Yu D, *et al.* Tian et al. reply. Nature, 2013, 502: E2–E3
34 Chaudhri MM, Lim YY. Harder than diamond? Just fiction. Nat Mater, 2005, 4: 4
35 Sumiya H, Ishida Y, Arimoto K, *et al.* Real indentation hardness of nano-polycrystalline cBN synthesized by direct conversion sintering under HPHT. Diamond Related Mater, 2014, 48: 47–51
36 Brookes CA, Moxley B. A pentagonal indenter for hardness measurements. J Phys E-Sci Instrum, 1975, 8: 456–460
37 Corrigan FR, Bundy FP. Direct transitions among the allotropic forms of boron nitride at high pressures and temperatures. J Chem Phys, 1975, 63: 3812–3820

Acknowledgements We acknowledge the financial support of the National Natural Science Foundation of China (51472213, 51332005, 51572235, 51722209 and 51525205) and the National Key R&D Program of China. Zhao Z also acknowledges the 100 Talents Plan of Hebei Province (E2016100013), the Natural Science Foundation for Distinguished Young Scholars of Hebei Province of China (E2018203349), and the Key R&D Program of Hebei Province of China (17211110D). Luo K acknowledges China Postdoctoral Science Foundation (2017M620097).

Author contributions Zhao Z and He J conceived the project. Zhao Z, Luo K, Zhang Y, Yu D, and He J designed the experiments. Luo K prepared the differently-sized oBN precursors. Luo K, Zhang Y, and Yu D performed the HPHT experiments. Li B, Hu W, and Nie A performed TEM observations. Luo K, Zhang Y, Yu D, Gao Y, Xu B, and Tian Y performed XRD, Raman, hardness, and fracture toughness measurements. Luo K, Liu Y, Wen B, Zhou XF, Tian Y, and He J analyzed the data. Luo K, Zhang Y, Zhao Z, and He J co-wrote the paper. All authors discussed the results and commented on the manuscript. All authors have given approval to the final version of the manuscript.

Conflict of interest The authors declare no conflict of interest.

Kun Luo is a postdoctoral fellow at the School of Science, Yanshan University. He received his PhD degree from Yanshan University in 2017. His research interest includes the design and synthesis of novel metastable materials under HPHT.

Zhisheng Zhao is a professor at the College of Materials Science and Engineering, Yanshan University. He received his PhD degree from Yanshan University in 2012. His research interest focuses on the design and synthesis of novel metastable materials and theoretical calculation.

洋葱式氮化硼粒径对纳米孪晶立方氮化硼组织结构和性能的影响

罗坤[1,2†], 张洋[1,2†], 于栋利[1†], 李宝忠[1], 胡文涛[1], 刘永[2], 高宇飞[1], 温斌[1], 聂安民[1], 赵智胜[1*], 徐波[1], 周向锋[1], 田永君[1], 何巨龙[1*]

摘要 拥有极高硬度、韧性和稳定性的纳米孪晶立方氮化硼(nt-cBN)在材料领域备受关注. 前期研究表明, 在高温高压条件下以洋葱式氮化硼(oBN)为前驱物是合成nt-cBN的关键. 本文研究发现, 前驱物oBN的粒径变化会显著影响最终产物的组织结构和机械性能. 随着前驱物oBN的粒径从~320 nm减小到~90 nm, 合成的纳米结构块材的硬度从61 GPa逐渐提高到108 GPa. 表明大粒径的oBN拥有和普通六方氮化硼类似的平整、有序的外层结构, 这与小粒径的oBN纳米粒子中存在大量弯曲、褶皱的氮化硼原子层及高密度层错的结构特点形成鲜明对比; 大粒径oBN前驱物中的这些有序结构显著减少了最终产物中超细孪晶亚结构的含量, 从而导致相应产物硬度的下降. 本研究表明, 只有粒径足够小的oBN前驱物才能合成出拥有高密度超细纳米孪晶结构且性能优异的nt-cBN. 为进一步提高此类纳米孪晶材料的性能提供了一种切实可行的方案.

